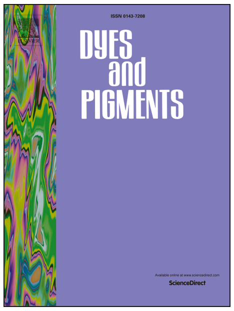

Synthesis, self-assembly, metal binding properties of triazole azobenzene based polycatenar dyes through click chemistry

Huiru Chen, Ruilin Zhang, Hongfei Gao, Huifang Cheng, Haipeng Fang, Xiaohong Cheng

PII: S0143-7208(17)31731-X
DOI: 10.1016/j.dyepig.2017.10.025
Reference: DYPI 6323

To appear in: *Dyes and Pigments*

Received Date: 11 August 2017
Revised Date: 25 September 2017
Accepted Date: 15 October 2017

Please cite this article as: Chen H, Zhang R, Gao H, Cheng H, Fang H, Cheng X, Synthesis, self-assembly, metal binding properties of triazole azobenzene based polycatenar dyes through click chemistry, *Dyes and Pigments* (2017), doi: 10.1016/j.dyepig.2017.10.025.

Graphical abstract

Synthesis, self-assembly, metal binding properties of triazole azobenzene based polycatenar dyes through click chemistry

Huiru Chen,[a]‡ Ruilin Zhang,[a,b]‡ Hongfei Gao,[a] Huifang Cheng,[a] Haipeng Fang,[a]
Xiaohong Cheng*[a]

[a] Key Laboratory of Medicinal Chemistry for Natural Resources, Chemistry School of Chemical Science and Technology, Yunnan University, Kunming, Yunnan 650091, P. R. China
Fax: (+86) 871 65032905
E-mail: xhcheng@ynu.edu.cn
[b] Forensic Medicine of Kunming Medical University, Kunming, Yunnan 650500, P. R. China
‡Both authors contributed equally to this work

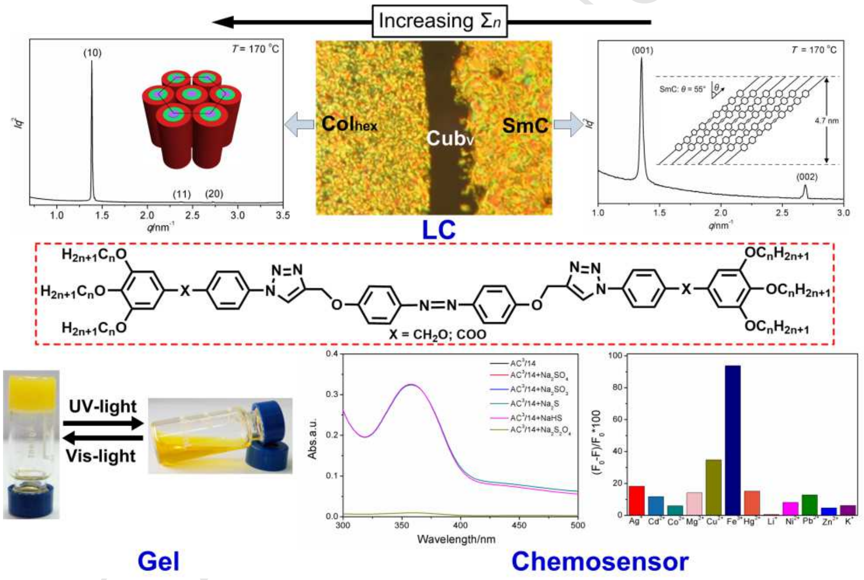

Synthesis, self-assembly, metal binding properties of triazole azobenzene based polycatenar dyes through click chemistry

Huiru Chen,[a]‡ Ruilin Zhang,[a,b]‡ Hongfei Gao,[a] Huifang Cheng,[a] Haipeng Fang,[a] Xiaohong Cheng*[a]

[a] Key Laboratory of Medicinal Chemistry for Natural Resources, Chemistry School of Chemical Science and Technology, Yunnan University, Kunming, Yunnan 650091, P. R. China
Fax: (+86) 871 65032905
E-mail: xhcheng@ynu.edu.cn
[b] Forensic Medicine of Kunming Medical University, Kunming, Yunnan 650500, P. R. China
‡Both authors contributed equally to this work

Abstract: Two series of novel polycatenar dyes consisting of a triazole azobenzene core were synthesized efficiently by copper-catalyzed azide-alkyne click (CuAAC) reaction. These compounds can self-assemble into SmC and $\mathrm{Col}_{hex}/p6mm$ liquid-crystalline phases, and form multistimuli responsive organogels. Bicontinuous cubic phase (Cub_V) could be induced in the binary system of a bicatenar compound with SmC phase and a hexacatenar compound with $\mathrm{Col}_{hex}/p6mm$ phase. Photophysical investigation indicates that these compounds have reversible photoresponsive properties in solution, liquid-crystalline and gel states. They can also act as chemosensors of Fe^{3+} and sodium dithionite with high selectivity.

Key words: Azobenzene; Liquid crystal; Photoresponsible behavior; Fluorescent chemosensor

1. Introduction

Liquid crystals (LCs) combining mobility and order on the molecular level have found wide application not only in electrooptical devices but also in molecular engineering nanotechnologies [1,2]. Novel mesogens by combination of different conjugated units such as azobenzene [3], heterocycles [4,5,6,7,8] into the skeletons of the classical liquid crystals have been reported in order to create advanced functional nanomaterials. Among them, azobenzene-based LCs have caused significant attention because the photoisomerization of the azobenzene provides a general way for the photocontrol of molecular structure and function [3]. Furthermore the azobenzene based LCs have found wide potentials as optoelectronic sensing devices [9] and organic light-driven actuators etc [10,11,12,13,14,15,16,17,18,19,20].

Polycatenar LCs consisting of a long aromatic rod-like core and multiple terminal flexible chains represent as a kind of nonconventional LCs [21,22,23,24,25,26,27]. Due to the nanosegregation of the aromatic rigid core and flexible chains, different LC phases like nematic, smectic (lamellar), bicontinuous cubic (Cub_V), columnar and even micellar cubic (Cub_I) phases depending on the number of the peripheral tails have been observed in such compounds. Cub_V phases, which represent intermediate states between lamellar and columnar organization, are interwoven 3D networks of channels, while Cub_I phases are formed by the regular organization of closed spheroidic aggregates, which have been reported in azobenzene-based [28], oligothiophene-based [29], and bent-shaped polycatenar LCs [30].

Click chemistry is an easy and fast access to create a diversity of structures applicable for pharmaceutical and material targets. The most representative “click chemistry” is copper-catalyzed azide-alkyne click (CuAAC) reaction [31,32,33], which can combine organic units into more complex architectures. The 1,2,3-triazole ring generated by the click chemistry has highly chemical and thermal stabilities, a good hydrogen-bond-accepting ability [34,35] as well as a nitrogen (N)-donor ability [36,37,38]. 1,2,3-triazole can enhance the molecular anisotropy when linear connected to other aromatic groups, meanwhile it can lead to an increase in the molecular dipole and dielectric anisotropy. Despite these advantages, the CuAAC reaction has only been used for synthesis of calamitic [39,40,41] or discotic liquid-crystalline materials [42,43], seldom for polycatenar LCs [30,44], and so far as we know there is no report on polycatenar liquid crystal combining azobenzene core with triazole wings.

We have recently reported novel amphotropic azobenzene derivatives [45], cholesterol-azobenzene dimesogens [46] which can display interesting properties such as photoinduced liquid crystalline phase and photoresponsive chiral amplification effect. Considering the useful properties and wide applications, photoswitchable azobenzene based polycatenars [28,47,48] have received little attention to date. Furthermore the mostly reported azobenzene based LCs contain the azo linkage either at the periphery [49,50,51] or only in a few cases at the central of the molecules [28,52,53].

Therefore herein to continue our interest in study the novel azobenzene mesogens, we report the facile synthesis and properties of series of novel polycatenar LCs $\mathbf{AC}^{\boldsymbol{m}}/\boldsymbol{n}$ and $\mathbf{AE}^{\boldsymbol{m}}/\boldsymbol{n}$ with an azobenzene core and 1,2,3-triazole units at both sides *via* the CuAAC click reaction. Alkoxy substituted phenyl units are attached at both terminals *via* acetate linkage (X = COO, series $\mathbf{AC}^{\boldsymbol{m}}/\boldsymbol{n}$) or ether linkage (X = CH_2O, series $\mathbf{AE}^{\boldsymbol{m}}/\boldsymbol{n}$). In the notation the letter ***m*** gives the number of alkoxy chains and the superscript ***n*** identifies the alkoxy chain length.

The effect of various linkages X as well as the number and length of the terminal alkyl chains on the self-assembly behavior of these compounds was investigated. Our study shows that these compounds can self-assemble into liquid crystalline phases in the bulk states and form multistimuli responsive organogels in organic solvents. They have reversible photoresponsive properties, and can act as chemosensor towards Fe^{3+} and sodium dithionite with high selectivity.

2. Experimental

2.1. Materials

The structures of the compounds are shown in Scheme 1. Reactions requiring an inert gas atmosphere were conducted under argon and the glassware was oven-dried (120 °C). Commercially available chemicals were used as received. The solvents were dried and distilled by conventional methods. ^{1}H-NMR and ^{13}C-NMR spectra were recorded on a Bruker-DRX-400 spectrometer with tetramethylsilane (TMS) as the internal standard. Elemental analysis was performed using an Elemental VARIO EL elemental analyzer. Thin-layer chromatography was performed on aluminum plates precoated with 5735 silica gel 60 PF254 (Merck). Column chromatography was performed on Merck silica gel 60 (230-400 mesh).

2.2. Methods and characterization

A mettler heating stage (FP 82 HT) was used for polarizing optical microscopy (POM, Optiphot 2, Nikon) and DSC were recorded with a DSC 200 F3 Maia calorimeter (NETZSCH). Their optical properties (UV-vis and fluorescent emission) were done on a UNIC UV2600A and HITACHI F-7000 spectrophotometers. SEM experiments were carried out on a QUNT200 scanning electron microscopy (SEM, USA). All pictures were taken digitally. For the sample preparation, the gel was placed on an aluminum foil paper for some time until the gel became dry gel, then the sample was gold plated, finally the sample was put into the scanning electron microscopy for observation.

Small-angle powder diffraction (SAXS) experiments were performed in transmission mode with synchrotron radiation at the 1W2A SAXS beamline at Beijing Accelerator Laboratory and the beamline BL16B1 at Shanghai Synchrotron Radiation Facility (SSRF). A modified Linkam hot stage with a thermal stability within 0.2 °C was used, with a hole for the capillary drilled through the silver heating block and mica windows attached to it on each side. Samples were held in the poly(imide) (Kapton) film. A MarCCD 165 detector was used. q calibration and linearization were verified using several orders of layer reflections from silver behemate.

For electron density reconstruction, fourier reconstruction of the electron density was carried out using the general formula for 2D periodic systems:

$$\rho_{xy} = \sum_{hk} \frac{1}{m_{hk}} \cdot |F_{hk}| \cdot \cos(\varphi_{hkl}) \cdot (\cos(2\pi \cdot (hx + ky))) \qquad (1)$$

here m being the multiplicity, F the structure factor, which is proportional to the intensity and φ the phase of the reflex.

2.3. Synthesis

Full synthesis scheme is shown in Scheme 1. 4-Azidophenol **1** [54], alkoxybenzoic acid **2^{m}/*n*** [55,56], alkoxybenzyl chlorides **3^{m}/*n*** [57,58], aryl azides **4^{m}/*n*** [59,60] and **5^{m}/*n*** [30], 4,4'-dihydroxyazobenzene **6** [61] and 4,4'-dipropargyloxyazobenzene **7** [62] were prepared according to literature procedures. A CuAAC click reaction between 4,4'-dipropargyl oxyazobenzene **7** and aryl azides **4^{m}/*n*** and **5^{m}/*n*** respectively to yield the target products **AC^{m}/*n*** and **AE^{m}/*n*** respectively. All products were purified using column chromatography. Experimental procedures and analytical data are collated in the Supporting Information (SI).

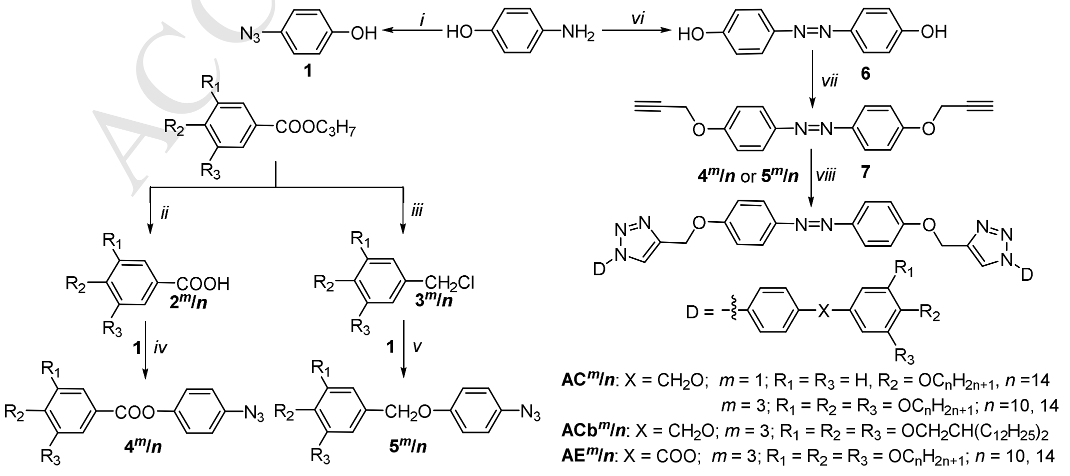

Scheme 1. Synthesis of the **ACb^{m}/*n***, **AC^{m}/*n*** and **AE^{m}/*n***, *Reagents and conditions*: *i*) a) $NaNO_2$, HCl, H_2O, 0 °C, 1

h; b) NaN_3, 0-5 °C, 12 h; *ii*) EtOH, KOH, 90 °C, 6 h; *iii*) a) $LiAlH_4$, THF, 0 °C, 2 h; b) $SOCl_2$, THF, RT, 2 h; *iv*) DCC, DMAP, DCM, RT, 12 h; *v*) NaH, THF, 70 °C, 20 h; *vi*) a) $NaNO_2$, HCl, H_2O, 0 °C, 1 h; b) phenol, NaOH, 0-5 °C, 12 h; *vii*) propargyl bromide, K_2CO_3, acetone, 50 °C, 12 h; *viii*) $CuSO_4 \cdot 5H_2O$, sodium ascorbate, TBA : H_2O = 1 : 1, THF, 40 °C, 12 h.

3. Results and discussion

3.1. Mesomorphic properties

Table 1 Transition temperatures, associated enthalpy values (in brackets) and X-ray data of compounds **AC^m/*n***, **AE^m/*n*** and **ACb^3/12**^{a}

Comp.	R_1, R_2, R_3	T/°C [ΔH/ kJ mol^{-1}]	a/nm (T/°C)	n
AC^1/14	$R_1 = R_3 = H$, $R_2 = OC_{14}H_{29}$	Cr 160 [103.62] SmC 186 [2.11] Iso	-	-
AC^3/10	$R_1 = R_2 = R_3 = OC_{10}H_{21}$	Cr 144 [68.29] Col_{hex} 177 [6.53] Iso	5.30(180)	3.9
AC^3/14	$R_1 = R_2 = R_3 = OC_{14}H_{29}$	Cr 142 [22.39] Col_h 165 [1.23] Iso	-	-
AE^3/10	$R_1 = R_2 = R_3 = OC_{10}H_{21}$	Cr 116 [26.38] Col_{hex} 162 [2.83] Iso	5.25(125)	3.9
AE^3/14	$R_1 = R_2 = R_3 = OC_{14}H_{29}$	Cr 116 [197.41] Col_{hex} 146 [4.40] Iso	5.55(140)	3.6
ACb^3/12	$R_1=R_2=R_3=OCH_2CH(C_{12}H_{25})_2$	Amorphous	-	-

^{a} Transition temperatures were determined by DSC (peak temperature from the first heating scan, at a rate of 5 K min^{-1} for **AC^3/10**, **AC^3/14**, **AE^3/10**, **AE^3/14**; 1 K min^{-1} for compounds **AC^1/14**). Abbreviations: Cr = crystal; SmC = smectic C phase; Col_{hex} = hexagonal columnar phase; Col_h = hexagonal columnar phase (assignment based only on optical investigations, no XRD performed; Iso = isotropic liquid. Abbreviations: a = lattice parameter determined by XRD; n = number of molecules in the cross section of a column in the Col_{hex} phases (with assumed height of 0.45 nm). For Col_{hex} phase: $n = (a^2/2)\sqrt{3}\,h(N_A/M)\rho$, N_A = Avogadro constant, M = molecular mass, assuming a density of ρ = 1 g/cm^3.

The LC self-assembly of compounds **AC^m/*n*** and **AE^m/*n*** were investigated by polarized optical microscopy (POM), differential scanning calorimetry (DSC) and X-ray diffraction (XRD). All target compounds except **ACb^3/12** exhibit enantiotropic (thermodynamically stable) LC phases. The phase transition temperatures and enthalpies of the azobenzene derivatives are listed in Table 1.

3.1.1 Compounds (AC^1/14, AC^3/n and AE^3/n) and their formation of smectic and columnar phases

The rod-like dicatenar compound **AC^1/14** with one tetradecoxy chain at each end displays a schlieren texture as typical for smectic C phase (Fig. 1a) [63]. The small-angle X-ray scattering (SAXS) of this smectic C phase (Fig. 1b) shows that two reflection peaks are in the small angle region with a ratio of $d_{001}/d_{002} \approx 2$, which confirms the smectic organization [1]. The layer spacing was calculated to be d = 4.7 nm at 170 °C (Table S1), while the molecular length L_{max} = 8.2 nm (calculated by the MM2 method [64] and assuming a molecule in the most stretched conformation with all-*trans* conformation for the alkyl chains [65]). The ratio of the layer spacing (d) and the molecule length (L_{max}) is 0.57, indicating a monolayer structure in the SmC phase where the fully extended molecules take the orientation with a tilt angle $\theta \approx 55°$ (calculated by the relationship $\cos\theta = d/L_{max}$) from the layer normal (the inset of Fig. 1b). The value of the tilt angle is consistent with those of the reported SmC phases [66,67].

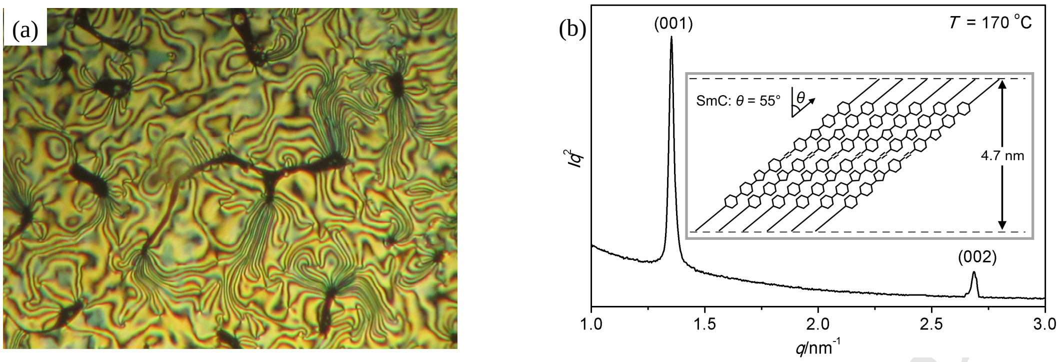

Fig. 1. SmC phase of compound **AC^1/14**: (a) texture as seen between crossed polarizers at T = 180 °C; (b) SAXS diffractogram at T = 170 °C; the inset shows the model of the molecular organization in monolayer of the SmC phase.

With increasing the number of the alkyl chains, all the other hexacatenar compounds **AC^3/*n*** (n = 10, 14) and **AE^3/*n*** (n = 10, 14) with 6 alkyl chains attached equally at each terminal display columnar mesophases. The columnar phases were identified by the typical spherulitic fan-like textures under POM. The investigations with an additional λ-plate under POM indicate that the columnar phases are optically negative (Fig. 2a and Fig. S1a-c). This means that the major intramolecular π-conjugation pathway, which is along the long axis of the aromatic cores, is perpendicular to the column long axis. The columnar phases were also investigated by SAXS. For compounds **AC^3/10**, **AE^3/10** and **AE^3/14**, there are three small angle reflections with a ratio of their reciprocal spacing 1: $3^{1/2}$: 2, which can be indexed to the 10, 11, 20 reflections of hexagonal lattice with $p6mm$ symmetry (Fig. 2b and Fig. S3-S4 and Table S2-S4). The number of molecules organized in a slice of the columns with a height of h = 0.45 nm (a typical value for the maximum of the diffuse wide angle scattering) n_{cell} could be calculated as shown in Table S5. Therefore it can be assumed that for these compounds approximately 4 molecules self-assemble into an overall disk-like stratum and they successively stack one another to form supramolecular columns, and these columns in turn self-organize to form a 2D parallelogram lattice (Fig. 2c), which was similar with the reported polycatenar mesogens [22]. The self-assembly model of $\mathrm{Col_{hex}}/p6\mathrm{mm}$ phase is in complete agreement with the reconstructed electron density map (Fig. 2d and Fig. S3b, S4b), where the high electron density areas (blue, purple) involving the azobenzene cores, which are surrounded by a medium electron density continuum (green) involving the benzylether groups, triazoles and some of the alkyl chains. The majority of the alkyl chains form the low electron density areas (red). It should be noted that the intermolecular π-π* interactions between the rod-like cores as well as nanosegregation of the aromatic center from the surrounding alkyl chain moieties would promote the assembly of these molecules into such columnar structures.

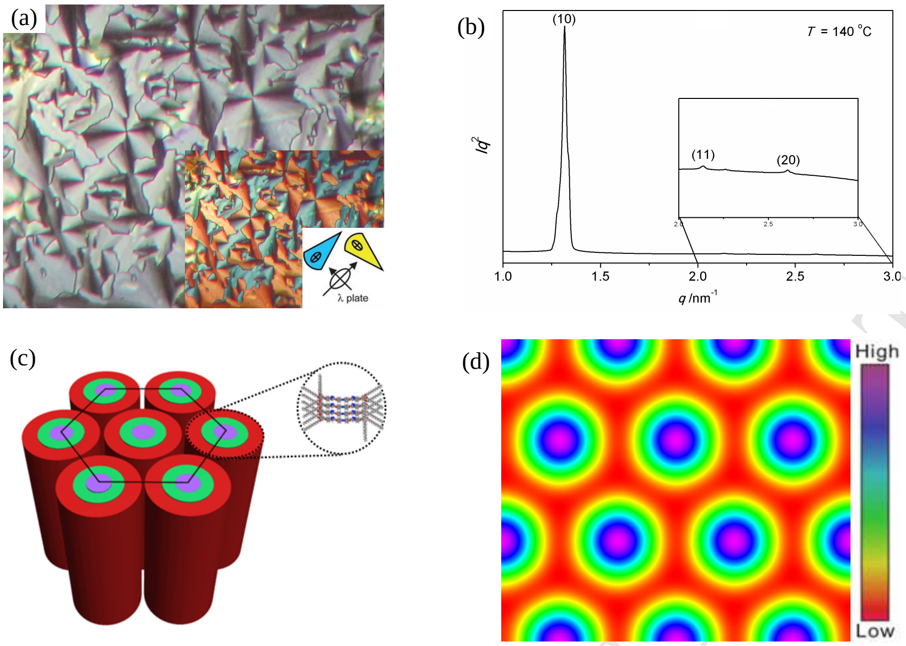

Fig. 2. Col$_{hex}$ phase of compound **AE^3/14**: (a) texture as seen between crossed polarizers at T = 130 °C, the inset shows the same region with λ-plate; (b) SAXS diffractogram at T = 140 °C; (c) the model showing the organization of compound **AE^3/14** in the Col$_{hex}$ phase; (d) electron density map as reconstructed from the diffraction pattern in (b), for the color code, see bar on the right.

Though the LC phase structure of compound **AC^3/14** was not characterized by SAXS, the investigations of the binary mixtures provided evidence that the columnar phase of **AC^3/14** is a hexagonal columnar phase too, just like that of **AE^3/14** (Fig. 3a). This was indicated by the continuous growth of the spherulitic texture of compound **AC^3/14** into the region of the Col$_{hex}$/*p*6*mm* phase of **AE^3/14** without any intermediate minimum, maximum, or visible miscibility gap [68].

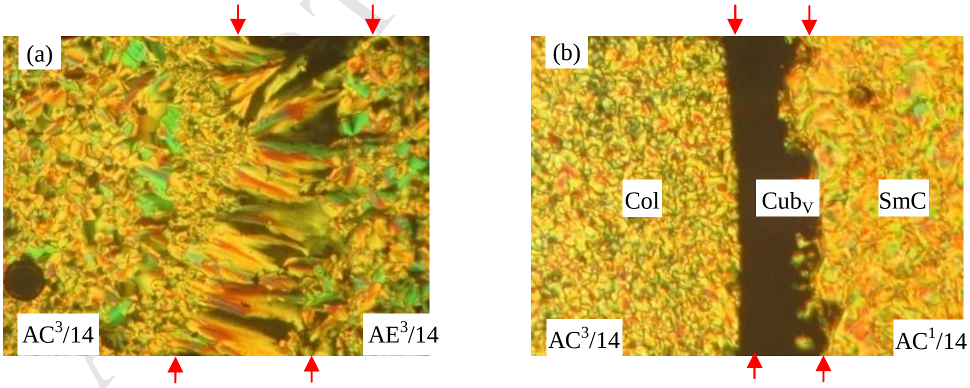

Fig. 3 (a) Contact region between the triangular honeycomb type LC phases of **AE^3/14** and **AC^3/14** at T = 142 °C; the dark areas represent the homeotropically aligned regions of the Col$_{hex}$/*p*6*mm* phases; the development of the contact region is shown in Fig. S5; (b) Contact region between **AC^3/14** and **AC^1/14** at T = 163 °C; The red arrows indicate the approximate position of the boundary between the two compounds.

Attempts to change the mesophase structure to the micellar cubic structure by the branching of the peripheral chains were unsuccessful. Compound **ACb^3/12** is completely isotropic and relatively viscous, but no cubic lattice could be found by XRD. There is only one diffuse scattering peak in the small angle range at about d = 4.19 nm (Fig. S6). Hence, the LC phase was completely lost, and additionally, no crystallization was observed. It appears that the chain branching leads to peripheral overcrowding, which distorts the core packing of the aromatics and destabilizes the ordered aggregates.

3.1.2 Binary mixture of different molecules

According to the thermotropic liquid-crystalline phase sequence formed by the polycatenar molecules [69], Cub_V phases could occur as intermediate phases between layer-like and columnar organization of these molecules with the increase of the interface curvature. In order to predict the possibility that the target molecules can self-assemble into Cub_V liquid-crystalline phase, we investigated the contact region between **AC^3/14** and **AC^1/14**. During the cooling process, an isotropic texture was observed in the contact region, which separated the spherulitic texture of **AC^3/14** and the schlieren texture of **AC^1/14** (Fig. 3b). The equal molar ratio binary mixture of **AC^3/14** and **AC^1/14** showed an isotropic mesophase in the temperature range of 125 °C-173 °C, which is consistent with the DSC trace of this binary mixture (Fig. S2f). The typical feature of the induced optically isotropic mesophase (viscoelasticty, supercool ability) is identified with those of the cubic mesophases of the pure compounds, confirmed its cubic phase nature. The self-assemble structure of this cubic phase needs to be further investigated by the SAXS experiment.

It is interesting to compare these triazole-azobenzene polycatenars with our previously reported polycatenar mesogen **IE^3/14** [30] (Fig. 4). It clearly shows that replacement of bisphenylmethane bent central core in **IE^3/14** with azobenzene leads to both higher melting and clearing temperatures, and prevention the formation of the cubic phase for herein reported triazole-azobenzene polycatenars **AE^3/14** and **AC^3/14**. The reduced flexibility of the azobenzene core in compounds **AE^3/14** and **AC^3/14** compared with the bisphenylmethane core in the reported compound **IE^3/14** should be responsible for these observations.

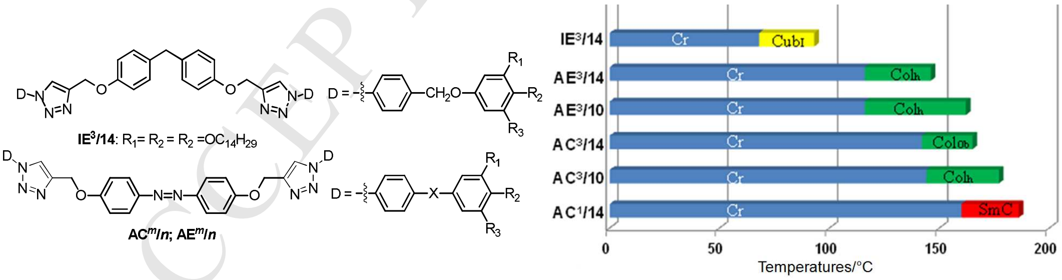

Fig. 4. Bar graph summarizing the thermal behavior of compounds **AC^m/*n***, **AE^m/*n*** under investigation and the reported compound **IE^3/14**.

Therefore the structure-LC property relationship of these triazole-azobenzene polycatenars focusing on the effects of the number, length and type of terminal alkyl chains as well as the type of linkage on their LC self-assembly behavior was systematically studied. In all cases, shearing the samples led to flow which removed the textures. This confirms the LC states of these materials. With increasing of the number of alkyl chains, the interface curvature between the nanosegregated regions of the triazole-azobenzene cores and the flexible chains should be increased. This structural variation results in the transition from the lamellar (SmC) phase for bicatenar compound to hexagonal columnar (Col_{hex}) phases for all hexacatenar compounds, which is similar to the mesomorphism of amphiphiles and block molecules [70], chain branching leads to none mesogenic material. It seems that it is difficult to achieve the Cub_I phase in these compounds, because of their long rigid cores.

All ether compounds **AE*^m^*/*n*** display broader range of mesophases with both reduced melting and isotropic temperature compared with the corresponding ester analogues **AC*^m^*/*n*** (Table 1). This should be attributed to less rigid and less polar ether group (X = CH_2O) contained in **AE*^m^*/*n*** compared with the carboxyl group (X = COO) contained in **AC*^m^*/*n***.

3.2. Photoisomerization behavior in liquid crystalline and solution

All the liquid-crystalline phases can respond to the UV irradiation immediately by change their textures to isotropic state and recovery to their LC textures after removing the UV light (Fig. 5 and Fig. S7). For example, compound **AC^1/14** was cooled from the isotropic liquid state to 170 °C in the range of the SmC phase (Fig. 5a). It was found that a phase transition from the SmC phase to the isotropic phase was realized in just 10 s under UV irradiation (Fig. 5b). Then the UV light was turned off after 15 s (Fig. 5c), schlieren textures of a typical SmC appeared again. It was believed that azo isomerization *trans-cis* disrupted the schlieren structure of the SmC phase, thus an order-decreasing phase transition was realized. It seems that the *trans-cis* photoisomerization effect on the liquid-crystalline property of the compounds reported here is very strong.

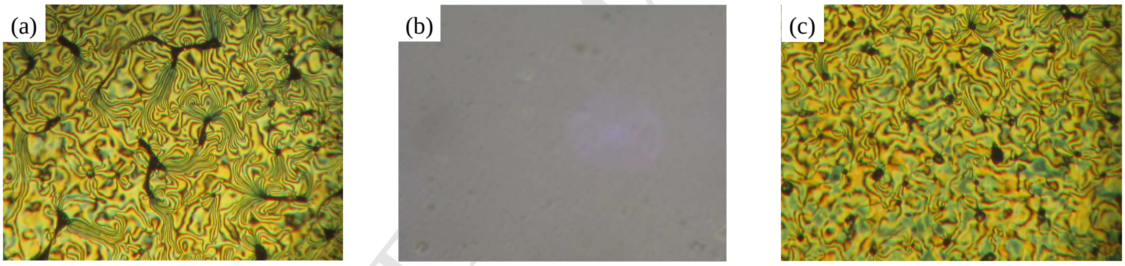

Fig. 5. Textural changes as observed by POM at the photoinduced SmC-Iso transition and the relaxation Iso-SmC as observed for compound **AC^1/14** at 170 °C: (a) before UV irradiation; (b) after UV irradiation for 10 s; (c) after visible light irradiation for 15 s.

The possible photochemical switching process of SmC-Iso reversible transition of **AC^1/14** is schematically represented in Fig. 6. Similarly, the compound **AE^3/14** showed photoisomerization reversible transition of Col-Iso (Fig. S7). Such photoisomerizations could be useful for light sensitive displays or data storage applications [45,46].

Additionally, such compounds exhibit the expected reversible *trans-cis* photoresponsive behavior in solution (Fig. S8-S12). The *trans-cis* transition under UV light irradiation led to a decrease of the π-π* band at 355 nm and an increase of the n-π* band at 450 nm, while the reverse *trans-cis* transition under visible light irradiation led to an increase of the absorption at around 355 nm and a decrease at around 450 nm. For these compounds, under the irradiation of 365 nm UV light of its CH_2Cl_2 solution (1×10^{-5} mol L^{-1}), the *trans-cis* transition was completely achieved about 120 s. Under visible light, the reverse *trans-cis* transition process was achieved within 240s.

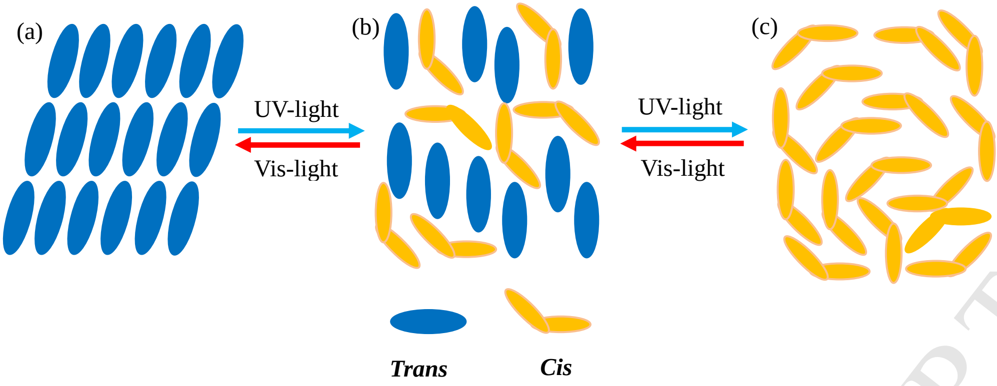

Fig. 6. Schematic illustration of the possible photochemical switching process in **AC^1/14**: (a) SmC phase; (b) SmC-Iso transition; (c) isotropic phase.

3.3. UV sensor property towards $Na_2S_2O_4$

Sodium dithionite ($Na_2S_2O_4$) is an important reducing agent in the textile and pulp industry. The azobenzene could exhibit reactivity toward $Na_2S_2O_4$ by cleaving the -N=N- bond to the phenylamine group [71,72]. As shown in Fig. 7a, A**C^3/14** had a yellow color in THF/H_2O solution (3:1, v/v at room temperature), and turned to pale and finally colorless after addition of the $Na_2S_2O_4$ solution, indicating the cleavage of azobenzene moiety. The chemical reaction was monitored by UV absorption spectra (Fig. 7b), which shows an intense absorption peak at 357 nm owing to the π-π* absorption of *trans*-azobenzene. Time-dependent UV absorption spectra shows that, with the addition of $Na_2S_2O_4$ solution, the UV absorption peak at 356 nm slowly disappeared and the cleavage reaction almost finished in 10 min (Fig. 7b). We also studied the reactivity of A**C^3/14** with other sulfur-carrying ions such as Na_2SO_4, Na_2SO_3, Na_2S and NaHS, which are the major interferents for sodium dithionite detection. The UV absorption spectra of A**C^3/14** solutions did not show obvious change, revealing the good selectivity of this reaction towards $Na_2S_2O_4$ (Fig. 7c). Therefore A**C^3/14** shows high reactivity toward $Na_2S_2O_4$, which providing a potential sodium dithionite sensor.

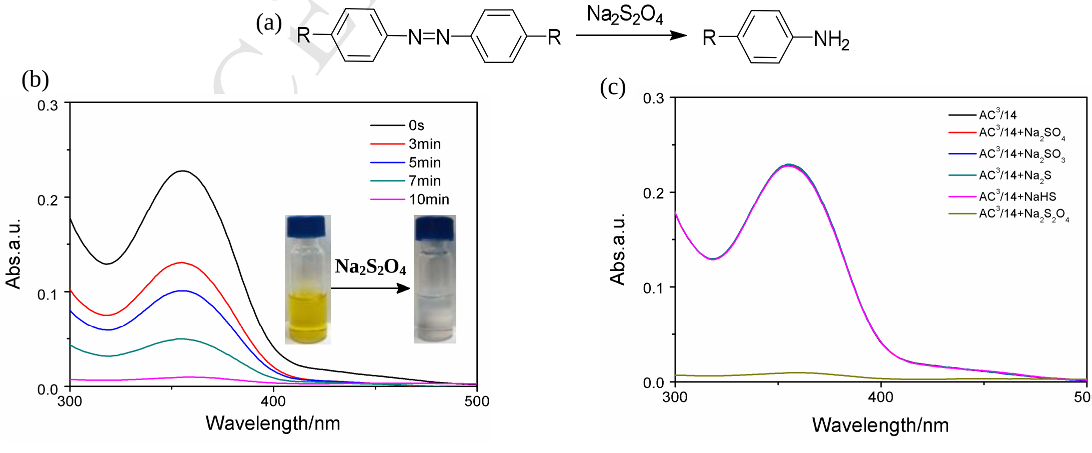

Fig. 7. (a) Schematic demonstration of compound **AC^3/14** reaction with $Na_2S_2O_4$ and the corresponding photos; (b) Time-dependent UV absorption spectra of **AC^3/14** solution(1×10^{-5} mol L^{-1}) in the presence of $Na_2S_2O_4$ (1×10^{-3} mol L^{-1}); (c) UV absorption spectra of **AC^3/14** solution (1×10^{-5} mol L^{-1}) in the presence of Na_2SO_4, Na_2SO_3, Na_2S, NaHS and $Na_2S_2O_4$ (1×10^{-3} mol L^{-1}).

3.4. Absorption and emission properties

The UV-vis absorption and fluorescence spectroscopic data of the chosen representative compounds **AC^1/14**, **AC^3/14**, **AE^3/14** in THF solution are shown in Fig. 8. These compounds show the maximum absorption peak at about 355 nm and the maximum emission peak around 402 nm in THF solution, which may be attributed to the π-π* transition. The absorption and fluorescence spectra of all these compounds in solutions show similar profiles, indicating that the molecular transmittance is mainly due to the azobenzene conjugate bridge structures in chromophores [73].

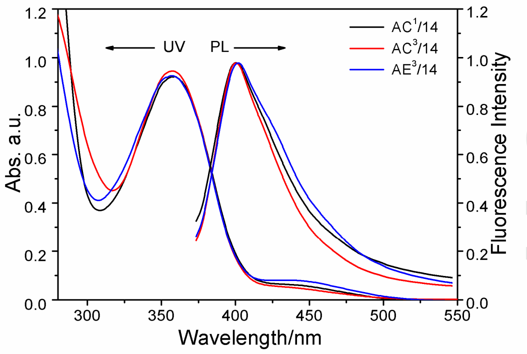

Fig. 8. Absorptions and fluorescence spectra of compounds **AC^1/14**, **AC^3/14** and **AE^3/14** in THF (1×10^{-6} mol L^{-1}).

For further investigation of the influence of solvent polarity on the optical properties of the compound of **AC^3/14**, the UV-vis and fluorescence spectra were measured in various solvents (Fig. 9). The main peaks of their absorption spectra locate at about 355 nm, which have very little changes in different organic solvents (Fig. 9a). With the increasing of the polarity of the solvents, the emission peaks showed only slightly red-shifted from about 392 nm (hexane) to about 414 nm ($CHCl_3$) (Fig. 9b). The Stokes shifts found to be 40, 44, 51 and 55 nm for cyclohexane, DCM, THF and $CHCl_3$ respectively (Table S6). Little influence of the solvent polarity on the optical properties of these compounds means that weak intramolecular charge transfer (ICT) exists in these molecules. The conformation and electron distributions of **AC^m/*n*** and **AE^m/*n***, calculated based on density functional theory (DFT) with the Gaussian 03W program package at B3LYP/(6-31G, d) level with the model compound **AC^3/14**, having methoxy groups instead of the $OC_{14}H_{29}$ chains indicate that the electron distributions of the HOMO and LUMO of **AC^3/14** are all located on the central phenyl moiety and azo groups (Fig. S13). This corresponds with weak ICT effect existing in these compounds deduced from the weak solvent effect.

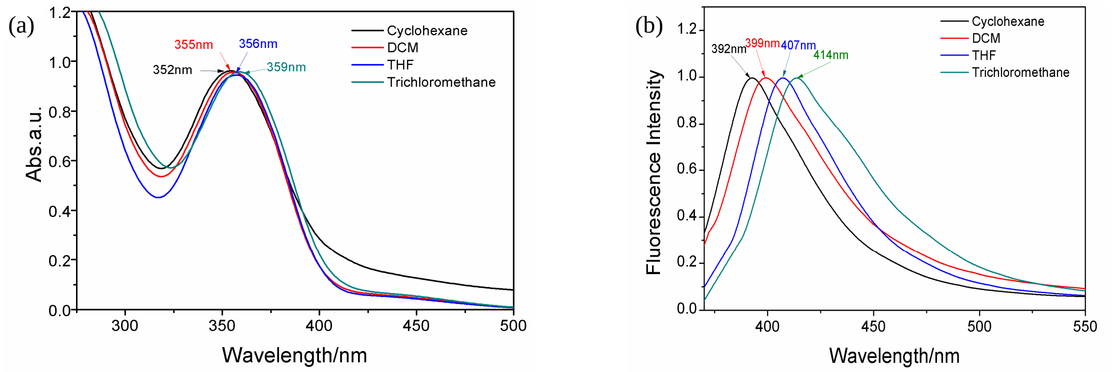

Fig. 9. (a) UV-vis spectra of **AC^3/14** (1×10^{-6} mol L^{-1}) at 20 °C in cyclohexane, DCM, THF, trichloromethane; (b) fluorescence spectra of **AC^3/14** (1×10^{-6} mol L^{-1}) in cyclohexane, DCM, THF, trichloromethane excited at 350 nm, 355 nm, 355 nm, 360 nm respectively.

3.5. Gelation properties

The gelation ability of these compounds was tested in various organic solvents at a concentration of 3.0 mg mL^{-1}. Among the synthesized polycatenars, only hexacatenar compounds **AC^3/14** and **AE^3/14** can form yellow gels in 1,4-dioxane and cyclohexane, and the results are summarized in Table 2. The bicatenar **AC^1/14** and other hexacatenars with short or branching alkyl chains have no gelation properties. These results indicate that the number or the length of terminal alkyl chains influences the gelation properties. This is probably due to the presence of alkyl chains maintaining the subtle balance between solubility and precipitation of the gelator molecules in a given solvent and also facilitating van del Waals interaction of gelator molecules [74]. Yellow gels could be obtained by cooling the heated solution of **AC^3/14** or **AE^3/14** quickly below 20 ºC or slowly down to room temperature.

The scanning electron microscopy (SEM) images of the xerogels formed by **AC^3/14** and **AE^3/14** are significantly different. For ester compound **AC^3/14**, its xerogel from polar solvent of 1,4-dioxane (Fig. 10 left) shows the formation of three-dimensional networks composed of twisted nanobelts. The approximate width of the nanobelt is 0.56-0.60 μm, and the length is more than 3.0 μm. While xerogel of **AC^3/14** from less polar solvent of cyclohexane shows the formation of the less ordered plate aggregates (Fig. S14a). In contrary, xerogel of ether compound **AE^3/14** from polar solvent of 1,4-dioxane shows the porous three-dimensional networks composed of entangled fibrous aggregates (Fig. S14b), while the unordered lump aggregates are observed in the xerogel of **AE^3/14** from less polar solvent of cyclohexane (Fig. S14c). Therefore gels from the more ploar solvent of 1,4-dioxane solvent displayed more ordered three-dimensional networks than gels form less polar solvent of cyclohexane, which displayed only less ordered plate or lump aggregates. The reason is that in polar solvents, the dipolar-dipolar interaction between polar solvents and triazole or azo units, as well as other non-covalent interactions such as π-π interaction, hydrogen bonding between the triazole or azobenzene units etc, all could drive the gel formation. Additionally, the more polar ester linkages in **AC^3/14** lead to stronger π-π interaction, therefore the formation of more ordered gel structure is observed for ester compound **AC^3/14** as compared with the ether compound **AE^3/14**.

Table 2 Gelation properties of **AC^3/14** and **AE^3/14**^{a}

Solvent	**AC^3/14**	**AE^3/14**	Solvent	**AC^3/14**	**AE^3/14**
THF	S	S	CH_2Cl_2	S	S
Ethyl acetate	S	S	Cyclohexane	G	G
Hexane	P	P	Ethanol	P	P
Methanol	P	P	*n*-Butanol	P	P
Acetone	P	S	Toluene	S	S
1,4-Dioxane	G	G	CH_3CN	P	P

^{a} S = solution, P = precipitation, G = gelation, gels formed at room temperature (20 ºC).

The organogels exhibit multiple stimuli-responsive behavior namely gel-sol reversible *trans* process upon exposure to a number of environmental stimuli including light, temperature, and shear etc (Fig. 10 right). Irradiation with UV light, application of heat or shear resulted in a sol state through disruption of the non-covalent interactions between the molecules, and the gel state can be recovered by the removal of such stimuli. Such multiple stimuli-responsive behaviors could be useful for delivery vehicles of small drug molecules [75], energy transfer [76], hardeners of solvents and sensors etc [77].

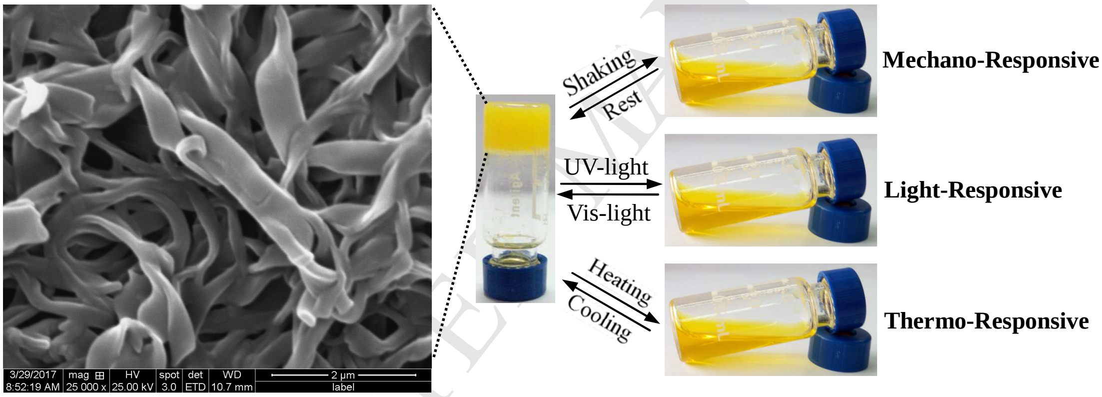

Fig. 10. SEM images of xerogel formed by **AC^3/14** in 1,4-dioxane and the scale bar is 2 μm (left); multistimuli responsive organogels formed by compound **AC^3/14** in 1,4-dioxane (3.0 mg mL^{-1}) (right).

3.6. Chemosensor behavior

Recently considerable efforts have been devoted to the development of chemosensors for the selective detection of heavy metal ions of environmental and biological importance. Among the heavy and transition metal ions, Fe^{3+} as a physiologically important metal ion, plays a catalytic role in chemical and biological processes such as oxygen metabolism and electron transfer, and both its deficiency and excess in the human body can induce a variety of diseases [78,79]. The 1,2,3-triazole motif introduced by click chemistry has its potential binding ability to transition metalions [80,81]. Hence, We have investigated the binding properties of **AC^m/*n*** for metal ions in THF : H_2O = 1 : 1, such as Ag^+, Cd^{2+}, Mg^{2+}, Fe^{3+}, Hg^{2+}, Li^+, Cu^{2+}, Pb^{2+}, Zn^{2+}, Ni^+, Co^{2+}, K^+. The result of the representative compound A**C^3/14** is shown in Fig. 11. During the addition of Fe^{3+}, the fluorescence intensity was dramatically decreased, which was the most significant change in fluorescence signals compared with the other metal ions.

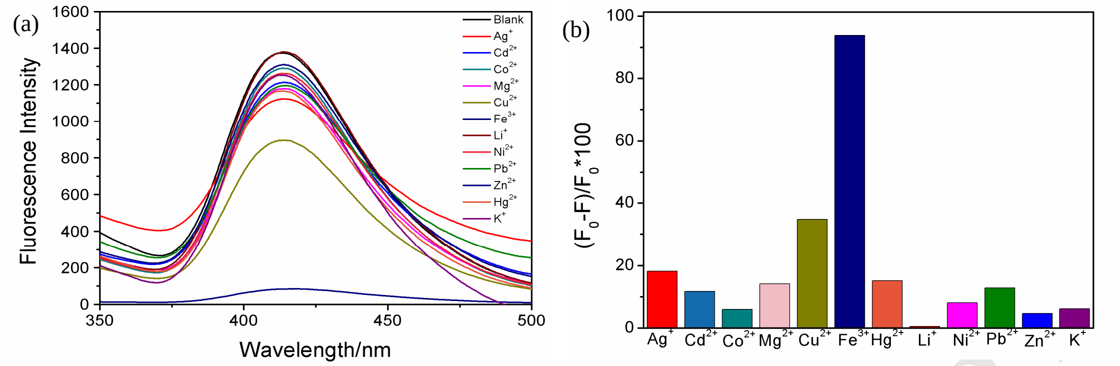

Fig. 11. Fluorescence spectra of compound **AC^3/14** (1×10^{-6} mol L^{-1}) in the presence of different metal ions (1×10^{-5} mol L^{-1}) at room temperature, all anions are ClO_4^-, at pH = 7.0. (a, b) THF: H_2O = 1 : 1 (λ_{ex} = 355 nm); $(F_0\text{-}F)/F_0\times100$ depicts the cation selective fluorescence quenching efficiency of compound **AC^3/14** namely the fluorescence responses of different metal ions; abbreviation: F_0 = the fluorescence emission maximum of blank sample; F = the fluorescence emission maximum of samples with addition of different metal ions.

We also performed the selectivity study on Fe^{3+}. In fluorescence spectra, an emission band centered at 415 nm appears upon addition of Fe^{3+} (from 0 to 25 equiv), and the emission intensity decreased linearly with $[Fe^{3+}]_{total}$. Nearly 10 equiv of metal ions being required for the saturation of the fluorescence intensity under the titration conditions, which was the most significant change in fluorescence signals compared with the other metal ions (Fig. 12) [82]. To further determine the sensitivity level, the detection limits [83,84] was ascertained to be 7.88×10^{-7} mol L^{-1} based on a 3σ/slope analysis under these experimental conditions (Fig. S15). By comparison, the detection limits of these compounds are lower than those of the reported compounds with two triazole units [85]. Therefore, compound **AC^3/14** could be used as a highly sensitive fluorescent chemosensor for the detection of Fe^{3+} in THF aqueous solution.

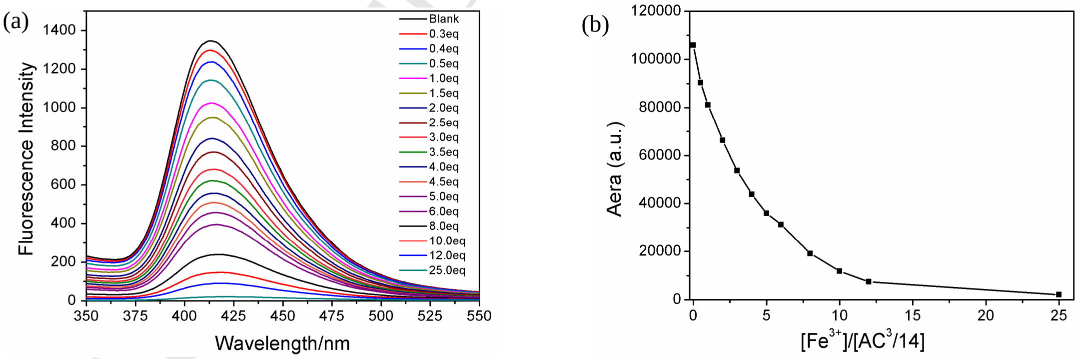

Fig. 12. (a, b) Fluorescence spectra of compound **AC^3/14** (1×10^{-6} mol L^{-1}) at 20 °C upon addition of Fe^{3+} (from 0 to 25.0 equiv) in THF: H_2O = 1 : 1 (λ_{ex} = 355 nm).

4. Conclusion

Therefore, it is possible to construct of a multifunctional molecule by using small different functional tectons with different functions. The novel triazole-azobenzene polycatenars reported here can self-assemble into LC phases. The increase of the interface curvature by increasing the number of alkyl chain leads to a mesophase transition from SmC to hexagonal columnar phases.

In the contact region between the SmC phase of compound **AC^1/14** and hexagonal columnar phase of **AC^3/14**, a reversed bicontinuous cubic phase was induced. The structure-property relationship of these triazole-azobenzene polycatenars focusing on the effects of the number, length and type of terminal alkyl chains as well as the linking groups on the self-assembly into lamellar and columnar phases is systematically studied.

Additionally, these compounds can self-assemble into gels with different morphologies in different organic solvents. The azobenzene as photosensitive unit endowing these compounds with the reversible photoresponsive behavior in liquid crystalline, solution and gel states is well demonstrated. The high reactivity of azobenzene toward $Na_2S_2O_4$ makes these compounds to be a potential sodium dithionite sensor. Metal recognizing properties of triazole units lead to these compounds acting as Fe^{3+} fluorescence sensor among a series of metal cations in THF-H_2O solution. These multi functional polycatenar dyes should have great potentials in optical electronic, biological as well as medical areas.

Acknowledgement

This work was supported by National Natural Science Foundation of China (Nos. 21664015, 21364017, 21274119 and 21602195) and the Yunnan Provincial Department of Education Foundation (Nos. ZD2015001 and 2016FD008). We thank beamline 1W2A at Beijing Accelerator Laboratory and beamline BL16B1 at Shanghai Synchrotron Radiation Facility (SSRF), China. The calculations were performed with the support of the Yunnan University Supercomputer Center.

References

---

[1] Demus D, Goodby JW, Gray GW, Spiess HW, Vill V. Handbook of liquid crystal. VCH-Wiley, Weinheim, 1998.
[2] Goodby JW, Collings PJ, Kato T, Tschierske C, Gleeson HF, Raynes P. Handbook of liquid crystals. VCH-Wiley, Weinheim, 2014.
[3] Bisoyi HK, Li Q. Light-driven liquid crystalline materials: From photo-induced phase transitions and property modulations to applications. Chem Rev 2016; 116: 15089-166.
[4] Zhang HC, Shiino S, Shishido A, Kanazawa A, Tsutsumi O, Shiono T, Ikeda T. A thiophene liquid crystal as a novel π-conjugated dye for photo-manipulation of molecular alignment. Adv Mater 2000; 12: 1336-39.
[5] O'Neill M, Kelly SM. Liquid crystals for charge transport, luminescence, and photonics. Adv Mater 2003; 15: 1135-46.
[6] Park YS, Kim D, Lee H, Moon B. Donor-acceptor-donor-type liquid crystal with a pyridazine core. Org Lett 2006; 8: 4699-702.
[7] Seed A. Synthesis of self-organizing mesogenic materials containing a sulfur-based five-membered heterocyclic core. Chem Soc Rev 2007; 36: 2046-69.
[8] Roy B, De N, Majumdar KC. Advances in metal-free heterocycle-based columnar liquid crystals. Chem Eur J 2012; 18: 14560-88.
[9] Lee SC, Lee SH, Kwon OP. Photoactive conducting polymers with light-driven conductivity modulation: Dual functionality for simple circuits. J Mater Chem C 2016; 4: 1935-44.
[10] Ikeda T, Mamiya J, Yu Y. Photomechanics of liquid-crystalline elastomers and other polymers. Angew Chem Int Ed 2007; 4: 506-28.
[11]Fleischmann EV, Zentel R. Liquid-crystalline ordering as a concept in materials science: From semiconductors to stimuli-responsive devices. Angew Chem Int Ed 2013; 52: 8810-27.
[12] Nakano M, Ikeda T. Photomechanics: directed bending of a polymer film by light. Nature 2003; 425: 145.
[13] Yu Y, Nakano M, Shishido A, Shishido T, Ikeda T. Effect of cross-linking density on photoinduced bending behavior of oriented liquid-crystalline network films containing azobenzene. Chem Mater 2004; 16: 1637-43.
[14] Kondo M, Yu Y, Ikeda T. How does the initial alignment of mesogens affect the photoinduced bending behavior of liquid-crystalline elastomers? Angew Chem Int Ed 2006; 45: 1378-82.
[15] Yu YL, Maeda T, Mamiya J, Ikeda T. Photomechanical effects of ferroelectric liquid-crystalline elastomers containing azobenzene chromophores. Angew Chem Int Ed 2007; 46: 881-3.
[16] Zhang YY, Xu J, Cheng F, Yin R, Yen CC, Yu Y. Photoinduced bending behavior of crosslinked liquid-crystalline polymer films with a long spacer. J Mater Chem 2010; 20: 7123-30.

[17] Ikeda T, Sasaki T, Ichimura K. Photochemical switching of polarization in ferroelectric liquid-crystal films. Nature 1993; 361: 428-30.

[18] Sasaki T, Ikeda T, Ichimura K. Photochemical control of properties of ferroelectric liquid crystals: Photochemical flip of polarization. J Am Chem Soc 1994; 116: 625-8.

[19] Coles HJ, Walton HG, Guillon D, Poetti G. Photomechanically induced phase transitions in ferroelectric liquid crystals. Liq Cryst 1993; 15: 551-8.

[20] Langhoff A, Giesselmann F. Photoferroelectric smectic-C* liquid crystal mixtures. Ferroelectrics 2000; 244: 283-93.

[21] Malthete J, Nguyen HT, Destrade C. Phasmids and polycatenar mesogens. Liq Cryst 1993; 13: 171-87.

[22] Nguyen HT, Destrade C, Malthete J. Phasmids and polycatenar mesogens. Adv Mater 1997; 9: 375-88.

[23] Rowe KE, Bruce DW. The synthesis and mesomorphism of di-, tetra- and hexa-catenar liquid crystals based on 2,2'-bipyridine. J Mater Chem 1998; 8: 331-41.

[24] Gharbia M, Gharbi A, Nguyen HT, Malthête J. Polycatenar liquid crystals with long rigid aromatic cores: A review of recent works. Curr Opin Colloid Interface Sci 2002; 7: 312-25.

[25] Alstermark C, Eriksson M, Nilsson M, Destrade C, Nguyen HT. Biforked mesogens with ester linkages, derived from 3-(3,4-dialkoxyphenyl)-propanoic acid. Liq Cryst 1990; 8: 75-80.

[26] Weissflog W, Wiegeleben A, Diele S, Demus D. Liquid crystalline swallow-tailed compounds I. Cryst Res Technol 1984; 19: 583-91.

[27] Weissflog W, Letko I, Diele S, Pelzl G. Mesomorphic behavior of new double swallow-tailed compounds. Adv Mater 1996; 8: 76-79.

[28] Peng XW, Gao HF, Xiao YL, Cheng HF, Huang FR, Cheng XH. Synthesis and self-assembly of photoresponsive and luminescent polycatenar liquid crystals incorporating an azobenzene unit interconnecting two 1,3,4-thiadiazoles. New J Chem 2017; 41: 2004-12.

[29] Yasuda T, Ooi H, Morita J, Akama Y, Minoura K, Funahashi M, Shimomura T, Kato T. π-Conjugated oligothiophene-based polycatenar liquid crystals: Self-organization and photoconductive, luminescent, and redox properties. Adv Funct Mater 2009; 19: 411-9.

[30] Cheng HF, Zhang RL, Li TH, Peng XW, Xia M, Xiao YL,Cheng XH. Synthesis and self assembly of bent core polycatenar mesogens with binding selectivity to Hg^{2+}. New J Chem 2017; 41: 8443-50.

[31] Tornøe CW, Meldal M. Peptidotriazoles: Copper(I)-catalyzed 1,3-dipolar cycloadditions on solid-phase. Springer Netherlands. 2001.

[32] Tornøe CW, Christensen C, Meldal M. Peptidotriazoles on solid phase: [1,2,3]-triazoles by regiospecific copper(I)-catalyzed 1,3-dipolar cycloadditions of terminal alkynes to azides. J Org Chem 2002; 67: 3057-64.

[33] Rostovtsev VV, Green LG, Fokin VV, Sharpless KB. A stepwise huisgen cycloaddition process: Copper(I)-catalyzed regioselective "ligation" of azides and terminal alkynes. Angew Chem Int Ed 2002; 41: 2596-99.

[34] Tome AC, Storr RC, Gilchrist TL. Science of synthesis, ed. Thieme, New York, 2004, vol. 13, p. 415.

[35] Krivopalov VP, Russ Shkurko OP. 1,2,3-Triazole and its derivatives. Development of methods for the formation of the triazole ring. Russ Chem Rev 2005; 74: 339-79.

[36] Mendoza-Espinosa D, Negron-Silva GE, Angeles-Beltran D, Alvarez-Hernandez A, Suarez-Castillo OR, Santillan R. Copper(II) complexes supported by click generated mixed *NN*, *NO*, and *NS* 1,2,3-triazole based ligands and their catalytic activity in azide-alkyne cycloaddition. Dalton Trans 2014; 43: 7069-77.

[37] Saleem F, Rao GK, Kumar A, Mukherjee G, Singh AK. Half-sandwich ruthenium(II) complexes of click generated 1,2,3-triazole based organosulfur/-selenium ligands: Structural and donor site dependent catalytic oxidation and transfer hydrogenation aspects. Organometallics 2013; 32: 3595-603.

[38] Struthers H, Spingler B, Mindt TL, Schibli R. "Click-to-Chelate": design and incorporation of triazole-containing metal-chelating systems into biomolecules of diagnostic and therapeutic interest. Chem Eur J 2008; 14: 6173-83.

[39] Vieira AA, Cristiano R, Bortoluzzi AJ, Gallardo H. Luminescent 2,1,3-benzothiadiazole-based liquid crystalline compounds. J Mol Struct 2008; 875: 364-71.

[40] Gallardo H, Bortoluzzi AJ, Santos DMPDO. Synthesis, crystalline structure and mesomorphic properties of new liquid crystalline 1,2,3-triazole derivatives. Liq Cryst 2008; 35: 719-25.

[41] Gallardo H, Bortoluzzi AJ, Conte G. Applying click chemistry to synthesis of chiral [1,2,3]-triazole liquid crystals. Liq Cryst 2005; 32: 667-71.

[42] Beltran E, Serrano JL, Sierra T, Gimenez R. Tris(triazolyl)triazine via click-chemistry: A C_3 electron-deficient core with liquid crystalline and luminescent properties. Org Lett 2010; 12: 1404-07.

[43] Majumdar KC, De N, Roy B, Bhaumik A. Synthesis and mesophase characterisation of a series of new triazine-based disc- shaped molecules. Liq Cryst 2010; 37: 1459-64.

[44] Choi JW, Han JH, Ryu MH, Cho BK. Oblique columnar assemblies of polycatenarmolecules via click chemistry. Bull Korean Chem Soc 2011; 32: 781-2.

[45] Tan XP, Zhang RL, Guo CX, Cheng XH, Gao HF, Liu F, Bruckner JR, Giesselmann F, Prehme M, Tschierske C. Amphotropic azobenzene derivatives with oligooxyethylene and glycerol based polar groups. J Mater Chem C 2015; 3: 11202-11.

[46] Tan XP, Li Z, Xia M, Cheng XH. Reversible photoresponsive chiral liquid crystal and multistimuli responsive organogels based on a cholesterol-azobenzene dimesogen. RSC Adv 2016; 6:20021-6.

[47] Alaasar M, Prehm M, Cao Y, Liu F, Tschierske C. Spontaneous mirror-symmetry breaking in isotropic liquid phases of photoisomerizable achiral molecules. Angew Chem Int Ed 2016; 55: 312-6.

[48] Alaasar M, Poppe S, Dong QS, Liu F, Tschierske C. Mirror symmetry breaking in cubic phases and isotropic liquids driven by hydrogen bonding. Chem Commun 2016; 52: 13869-72.

[49] Adachi H, Hirai Y, Ikeda T, Maeda M, Hori R, Kutsumizu S, Haino T. Photoresponsive toroidal nanostructure formed by self-assembly of azobenzene-functionalized tris(phenylisoxazolyl)benzene. Org Lett 2016; 18: 924-7.

[50] Yagai S, Yamauchi M, Kobayashi A, Karatsu T, Kitamura A, Ohba T, Kikkawa Y. Control over hierarchy levels in the self-assembly of stackable nanotoroids. J Am Chem Soc 2012; 134: 18205-8.

[51] Yagai S, Nakajima T, Kishikawa K, Kohmoto S, Karatsu T, Kitamura A. Hierarchical organization of photoresponsive hydrogen-bonded rosettes. J Am Chem Soc 2005; 127: 11134-9.

[52] Westphal E, Bechtold IH, Gallardo H. Synthesis and optical/thermal behavior of new azo photoisomerizable discotic liquid crystals. Macromolecules 2010; 43: 1319-28.

[53] Yan C, Xiao YL, Dai H, Cheng XH. Synthesis and properties of symmetric azobenzene derivative. Chem J Chinese U 2016; 37: 475-9.

[54] Hall JH, Fargher JM, Gisler MR. Substituent effects on spin delocalization in triplet phenylnitrenes.1. para-substituted phenylnitrenes. J Am Chem Soc 1978; 100: 2029-34.

[55] Cheng XH, Bai XQ, S Jing, Ebert H, Prehm M, Tschierske C. Self-assembly of imidazolium-based rodlike ionic liquid crystals: transition from lamellar to micellar organization. Chem Eur J 2010; 16: 4588-601.

[56] Seo SH, Park JH, Tew GN, Chang JY. Thermotropic liquid crystals of 1 *H*-imidazole amphiphiles showing hexagonal columnar and micellar cubic phases. Tetrahedron Lett 2007; 48: 6839-44.

[57] Müri M, Schuermann KC, Cola LD, Mayor M. Shape-switchable azo-macrocycles. Eur J Org Chem 2009; 15: 2562-75.

[58] Yoshio M, Kagata T, Hoshino K, Mukai T, Ohno H, Kato T. One-dimensional ion-conductive polymer films: Alignment and fixation of ionic channels formed by self-organization of polymerizable columnar liquid crystals. J Am Chem Soc 2006; 128: 5570-7.

[59] Beltran E, Serrano JL, Sierraa T, Gimenez R. Functional star-shaped tris(triazolyl)triazines: Columnar liquid crystal, fluorescent, solvatofluorochromic and electrochemical properties. J Mater Chem 2012; 22: 7797-05.

[60] Tan XP, Kong LY, Dai H, Cheng XH, Liu F, Tschierske C. Triblock polyphiles through click chemistry: Self-assembled thermotropic cubic phases formed by micellar and monolayer vesicular aggregates. Chem Eur J 2013; 19: 16303-13.

[61] Wei WH, Tomohiro T, Kodaka M, Okuno H. Selective synthesis and kinetic measurement of 1:1 and 2:2 cyclic compounds containing 1,4,7,10-tetraazacyclododecane and azobenzene units. J Org Chem 2000; 65: 8979-87.

[62] Casas-Solvas JM, Martos-Maldonado MC, Vargas-Berenguel A. Synthesis of β-cyclodextrin derivatives functionalized with azobenzene. Tetrahedron 2008; 64: 10919-23.

[63] Dierking I. Textures of liquid crystals. Wiley-VCH, Weinheim, 2003.

[64] *CAChe 3.2*, Oxford Molecular Ltd, Oxford, UK, 1999.

[65] Identical values were obtained with CPK models.

[66] Qu SN, Chen XF, Shao X, Li F, Zhang HY, Wang HT, Zhang P, Yu ZX, Wu K, WangY, Li M. Self-assembly of highly luminescent bi-1,3,4-oxadiazole derivatives through electron donor-acceptor interactions in three-dimensional crystals, two-dimensional layers and mesophases. J Mater Chem 2008; 18: 3954-64.

[67] Girotto E, Behramand B, Bechtold IH, Gallardo H. Thiophene-based bent-shaped luminescent liquid crystals: Synthesis and characterization. Liq Cryst 2017; 44: 1231-9.

[68] Gao HF, Cheng HF, Yang ZH, Prehm M, Cheng XH, Tschierske C. Synthesis and self-assembly of luminescent hexacatenar molecules incorporating a 4,7-diphenyl-2,1,3-benzothiadiazole core. J Mater Chem C 2015; 3: 1301-8.

[69] Tschierske C. Non-conventional liquid crystals-the importance of micro-segregation for self-organisation. J Mater Chem 1998; 8: 1485-508.

[70] Demus D, Goodby JW, Gray GW, Spiess HW, Vill V. Handbook of Liquid Crystals, ed. Wiley-VCH, Weinheim, 1998.

[71] Ma Y, Promthaveepong K, Li N. Chemical sensing on a single SERS particle. ACS Sens. 2017; 2: 135-9.

[72] Jaffe CL, Lis H, Sharon N. New cleavable photoreactive heterobifunctional cross-linking reagents for studying membrane organization. Biochemistry 1980; 19: 4423-9.

[73] Tang X, Jia K, Tang XZ, Chen L, Pan L. Effect of auxiliary electron-donating group on the microscopic nonlinear optical properties of vinyl and azobenzene based chromophores. J Mater Sci 2016; 27: 7174-82.

[74] Babu SS, Praveen VK. Ayyappanpillai A. Functional π-gelators and their applications. Chem Rev 2014; 114: 1973-2129.

[75] Friggeri A, Feringa BL, Esch JV. Entrapment and release of quinoline derivatives using a hydrogel of a low molecular weight gelator. J Controlled Release 2004; 97: 241-8.

[76] Praveen VK, George SJ, Varghese R, Vijayakumar C, Ajayaghosh A. Self-assembled π-nanotapes as donor scaffolds for selective and thermally gated fluorescence resonance energy transfer (FRET). J Am Chem Soc 2006; 128: 7542-50.

[77] Yang RM, Peng SH, Hughes TC. Multistimuli responsive organogels based on a reactive azobenzene gelator. Soft Matter 2014; 10: 2188-96.

[78] Swaminathan S, Fonseca AV, Alam GM, Shah VS. The role of iron in diabetes and its complications. Diabetes Care 2007; 30:1926-33.

[79] Crichton RR, Dexter DT, Ward RJ. Metal based neurodegenerative diseases-from molecular mechanisms to

therapeutic strategies. Coord Chem Rev 2008; 252: 1189-99.
[80] Bryant JJ, Bunz UHF. Click to bind: Metal sensors. Chem Asian J 2013; 8: 1354-67.
[81] Wu JD, Gao YX, Lu JR, Hu J, Ju Y. A steroid-coumarin conjugate for cascade recognition of copper ion and dihydrogen phosphate: microstructural features and IMPLICATION logic gate properties. Sens Actuators B 2015; 206: 516-23.
[82] Saleema M, Kang SK, Lee KH. Microwave assisted synthesis of a novel optical chemosensor for selective Fe^{3+} detection. J Lumin 2015; 162: 14-24.
[83] Yang L, Zhao H, Li Y, Zhang Y, Ye H, Zhao G, Ran X, Liu F, Li CP. Insights into the recognition of dimethomorph by disulfide bridged β-cyclodextrin and its high selective fluorescence sensing based on indicator displacement assay. Biosens Bioelectron 2017; 87: 737-44.
[84] Wang W, Wei J, Liu H, Liu Q, Gao Y. A novel colorimetric chemosensor based on quinoline for the sequential detection of Fe^{3+} and PPi in aqueous solution. Tetrahedron Lett 2017; 58: 1025-9.
[85] Chen KH, Lu CY, H. Cheng J, Chen SJ, Hu CH, Wu AT. A pyrenyl-appended triazole-based ribose as a fluorescent sensor for Hg^{2+} ion. Carbohydrate Research 2010; 345: 2557-61.

Polycatenar dyes consisting of a triazole azobenzene core have been successfully synthesized via click chemistry.

These polycatenar dyes can self-assemble into SmC and $\mathrm{Col_{hex}}/p6mm$ mesophases and organogels with different morphologies.

Bicontinuous cubic phase ($\mathrm{Cub_V}$) could be induced in the binary system of SmC phase and $\mathrm{Col_{hex}}/p6mm$ phase.

These polycatenar dyes exhibit reversible photoresponsive behavior in solution, liquid-crystalline states and gel states.

These polycatenar dyes can act as chemosensors of Fe^{3+} and $Na_2S_2O_4$ with high selectivity.